moistened with ethanol, or by gently sanding it with sandpaper (number 600).

Figure 3 is a lower magnification image of a gold film immersed in 2 m*M* NaCl. Our intent was to approximate the ionic concentration of a dilute solution of DNA. Images of this magnification were obtained routinely; we obtained more than 100 in a few days.

Gold depositions took place in a diffusion-pumped chamber at 5×10^{-6} torr. The cleaned glass substrate (a number 2 cover slide) was exposed for 30 seconds to glow discharge and then coated with a 7-Å chromium underlayer to improve adhesion of the gold film. The gold was evaporated from resistively heated sources and deposited at a rate of 3 Å per second to a thickness of 1000 Å, as measured by a quartz crystal thickness monitor.

The use of water as a medium did not complicate the operation of the tunneling microscope after the problem of operating in the presence of parallel conduction was solved. No evidence of the aqueous environment is evident from the images themselves. This is consistent with experimental results in air, liquid nitrogen, and paraffin oil (*9, 15*), in which the environment had no obvious effect on the images of the surface studied. Since the scan rate was slow compared to molecular motion, one would expect any effects due to water molecules in the gap to have been time-averaged.

In conclusion, a tunneling microscope can be operated in an aqueous environment and yield high-resolution images. This technique could be applied in several disciplines. In electrochemistry, it could be used to image an electrode surface before and after electrodeposition and, more generally, to study electrode reactions as a function of the structures on the electrode surface (*26*). In biology, the possibilities include imaging DNA, proteins, and membranes in their active states. If these were successful, further goals could include direct observation of biological processes such as DNA replication, enzymatic catalysis, and membrane transport.

REFERENCES AND NOTES

1. G. Binnig and H. Rohrer, *Surf. Sci.* **126**, 236 (1983).
2. ———, Ch. Gerber, E. Stoll, *ibid.* **144**, 321 (1984).
3. G. Binnig, H. Rohrer, Ch. Gerber, E. Weibel, *Phys. Rev. Lett.* **50**, 120 (1983).
4. J. A. Golovchenko, *Bull. Am. Phys. Soc.* **30**, 251 (1985).
5. R. M. Feenstra and G. S. Oehrlein, *Appl. Phys. Lett.* **47**, 97 (1985).
6. H. J. Scheel, G. Binnig, H. Rohrer, *J. Cryst. Growth* **60**, 199 (1982).
7. R. Miranda *et al.*, *Appl. Phys. Lett.* **47**, 367 (1985).
8. S. A. Elrod, A. L. de Lozanne, C. R. Quate, *Appl. Phys. Lett.* **45**, 1240 (1984).
9. R. V. Coleman, B. Drake, P. K. Hansma, G. Slough, *Phys. Rev. Lett.* **55**, 394 (1985).
10. A. M. Baró *et al.*, *Nature (London)* **315**, 253 (1985).
11. R. Hooke, *Micrographia* (London, 1665; reprinted by Weinheim, New York, 1961).
12. A. V. Leeuwenhoek, *Arcana Natura Detecta* (Leiden, 1772).
13. C. F. Quate, *Phys. Today* **38**, 34 (August 1985).
14. M. Howells, J. Kirz, D. Sayre, G. Schmahl, *ibid.*, p. 22.
15. B. Drake *et al.*, *Rev. Sci. Instrum.*, in press.
16. The material was called Grade ZYA Graphite Monochromator and was purchased from Union Carbide Corporation, Carbon Products Division, Chicago, IL.
17. A. L. Robinson, *Science* **220**, 43 (1983).
18. ———, *ibid.* **225**, 1137 (1984).
19. G. Binnig and H. Rohrer, *Sci. Am.* **253**, 50 (August 1985).
20. Model 30-05-1, Frederick Haer & Co., Brunswick, ME.
21. G. Binnig *et al.*, *Europhys. Lett.* **1**, 31 (1986).
22. Sang-Il Park and C. F. Quate, *Appl. Phys. Lett.* **48**, 112 (1986).
23. P. K. Hansma, R. Sonnenfeld, J. Schneir, B. Drake, J. Hadzicki, *Bull. Am. Phys. Soc.* **30**, 309 (1985).
24. A. Selloni, P. Carnevali, E. Tosatti, C. D. Chen, *Phys. Rev. B* **31**, 2602 (1985).
25. J. Tersoff, in preparation.
26. A. T. Hubbard *et al.*, *J. Electroanal. Chem.* **168**, 43 (1984).

27. Supported by NSF grant DMR83-03623. We thank Ch. Gerber and G. Binnig for suggesting that it might be possible to use water, on the basis of their preliminary experiments with a drop, N. Garcia for suggesting a study of highly oriented pyrolytic graphite, and S. Lindsay for suggesting the use of a saline solution. We thank S. Alexander, D. Cannell, S. Chiang, B. Drake, H. Hansma, A. Hubbard, J. Israelchevili, M. Kullin, S. Morita, H. Rohrer, D. Salisbury, C. Schneiker, J. Schneir, and J. Tersoff for useful discussions and especially K. Dransfeld and C. Quate for their enthusiasm and encouragement.

23 December 1985; accepted 3 March 1986

Decrease in Deformation Rate Observed by Two-Color Laser Ranging in Long Valley Caldera

M. F. LINKER, J. O. LANGBEIN, A. MCGARR

After the January 1983 earthquake swarm, the last period of notable seismicity, the rapid rate of deformation of the south moat and resurgent dome of the Long Valley caldera diminished. Frequently repeated two-color laser ranging measurements made within a geodetic network in the caldera during the interval June 1983 to November 1984 reveal that, although the deformation accumulated smoothly in time, the rate of extension of many of the baselines decreased by factors of 2 to 3 from mid-1983 to mid-1984. Areal dilatation was the dominant signal during this period, with rates of extension of several baselines reaching as high as 5 parts per million per annum during the summer of 1983. Within the south moat, shear deformation also was apparent. The cumulative deformation can be modeled as the result of injection of material into two points located beneath the resurgent dome in addition to shallow right lateral slip on a vertical fault in the south moat.

DRAMATIC EPISODES OF RAPID crustal deformation (*1, 2*) and unusual patterns of seismicity and attenuation (*3*) demonstrate that Long Valley caldera, a center of rhyolitic and basaltic volcanism in eastern California (*4*) within a region of lithospheric extension (*5*), is a potential site for volcanic hazard (*6*). Because of the concern that continued crustal deformation may lead to a volcanic eruption (*7*), we installed a geodetic network with which to observe subtle changes in the pattern of deformation within the south moat and to a lesser degree across the resurgent dome (Fig. 1) by means of a portable two-color geodimeter (*8*). We present data from 707 measurements made in this network from June 1983 to November 1984 (*9*).

The dominant feature of the data (Fig. 2) is the substantial lengthening of most of the baselines. When averaged over the initial 4 months, the lengthening rates of five of the baselines exceeded 5 parts per million (ppm) per annum, which is more than an order of magnitude greater than typical rates observed along geodetic baselines in the environs of the San Andreas fault zone (*10, 11*).

Perhaps the most interesting aspect of the data is the reduction in the rate of deformation during the period of observation. This decrease can be seen readily on 6 of the 13 individual line-length time histories that sample the entire reporting period. These include Casa-Hot, Casa-Rodger, Casa-Lomike, Casa-Sewer, Miner-Tilla, and Miner-Shark (Fig. 2), whose rates of lengthening decreased by factors of 2 to 3 from mid-1983 to mid-1984. For these six baselines, the addition of quadratic terms to models of constant lengthening rate is statistically significant.

To characterize the spatial distribution of cumulative deformation, we estimated the net length change of those baselines for which sufficient data exist during the time interval mid-July 1983 to mid-August 1984. Table 1 lists the length changes together with the estimated standard deviations based on the conservative assumption that each length change is determined from only

U.S. Geological Survey, Menlo Park, CA 94025.

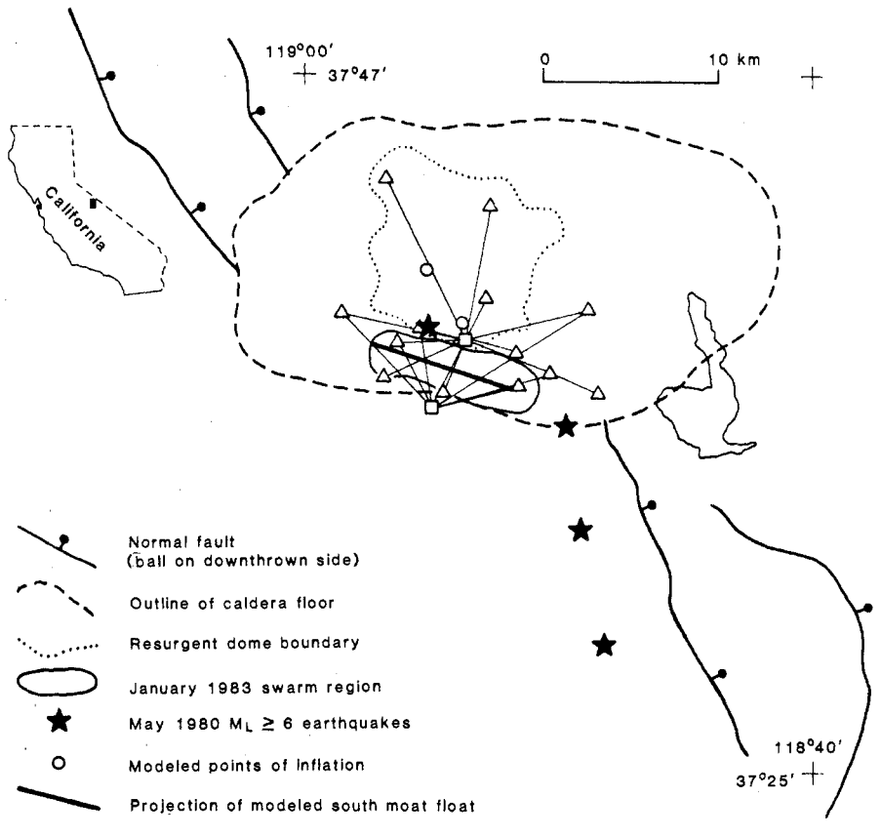

Fig. 1. Map showing key tectonic features of the Long Valley area, location of the four May 1980 earthquakes (local magnitude ≥ 6) and the January 1983 earthquake swarm, the two-color geodimeter network, and surface projections of sources used to model the geodetic data.

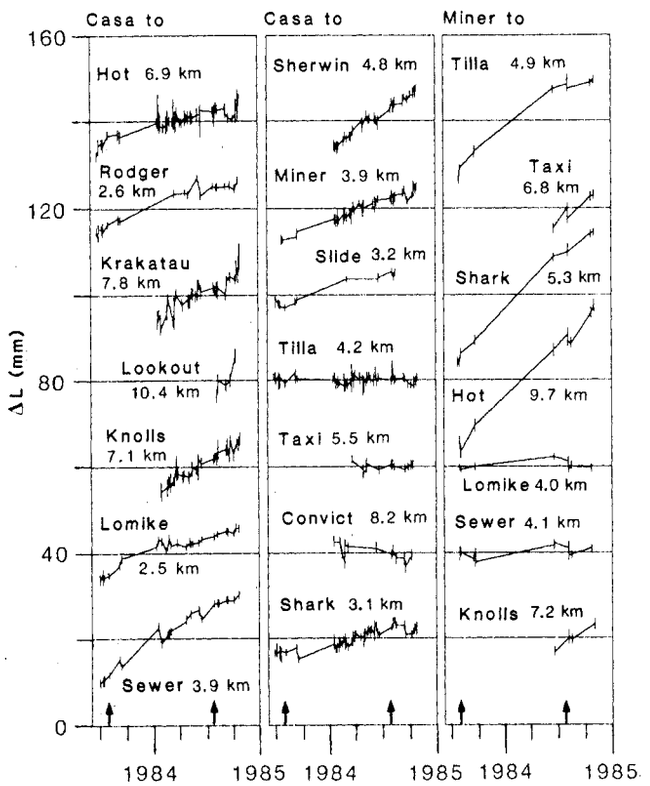

Fig. 2. Changes in line length (ΔL) as a function of time from data collected with the two-color geodimeter. The vertical axis is referenced to an arbitrary distance for each baseline. The baselines are arranged in the figure as they are azimuthally in the network about the two instrument stations, starting with east and progressing counterclockwise. The error bars represent one standard deviation of the error in the length measurements. The approximate lengths of the baselines are indicated adjacent to the data. The arrows indicate the times for the modeled interval, 20 July 1983 to 10 August 1984.

two measurements of each baseline given the previously described a priori error estimate for an individual datum. For Casa-Krakatau, -Knolls, and -Sherwin, three baselines that were not established until January 1984, we extrapolated from the data back in time to estimate their cumulative change in length. The error estimates for these three baselines are accordingly larger than those for the other 13 baselines. The length change for the baseline Casa-Lookout is taken from the Geodolite data of Estrem and co-workers (*12*).

After determining that the cumulative length change data (Table 1) could not be represented adequately by models involving spatially homogeneous strain changes (*10*), we constructed a map to represent the distribution of linear strain throughout the network (Fig. 3). Both the nonuniformity of strain and the predominance of extension are apparent in this map. The existence of steep gradients in the strain field is evident in the comparison of the baselines Miner-Shark to Miner-Hot and Casa-Shark to Casa-Lomike. All the baselines exhibit extension except a few of those that lie near or within the region of the January 1983 earthquake swarm. In particular, Casa-Tilla, Miner-Sewer, and Miner-Lomike all display little change. These anomalies in the otherwise pervasively dilatent field are qualitatively consistent with a strain field resulting from the presence of a zone of right lateral shear within the south moat superimposed on a more regional dilation, with the anomalous baselines positioned such that the sum of the two deformation fields results in almost no net length change.

To investigate the tectonic implications of these results, we developed a simple model from the two-color geodimeter data (Table 1) in conjunction with the Geodolite observations for the same time interval (*12*). As a starting point in the iterative process of searching for models that fit the combined data set, the model developed by Estrem and co-workers (*12*) for the Geodolite data alone (here termed model 1) was first tested against the observations and found to be unsatisfactory. Model 1 involves a single point source of dilatation beneath the resurgent dome 3 km north and 0.6 km east of station Casa at a depth of 10 km, plus right lateral slip on a vertical fault in the south moat in the depth interval 0 to 2 km. The inadequacy of model 1 with respect to the two-color data is not surprising because the two-color network samples the short wavelength complexities of the sources involved, in contrast to the observations from the much broader Geodolite network that extends across and beyond the caldera. The inferred location of the south moat fault with respect to stations Tilla and Sewer is

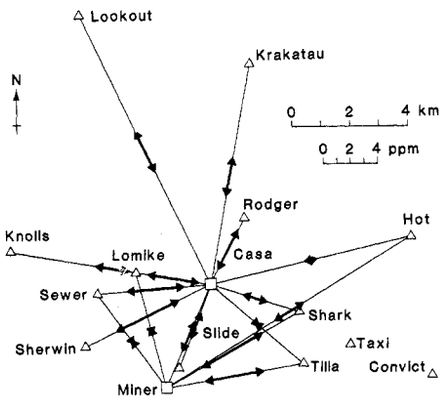

Fig. 3. Map of linear strain in the two-color network. The arrows, indicating the proportional lengthening of the individual baselines for the period 20 July 1983 to 10 August 1984, are plotted at the midpoints of their baselines. The changes in length of the baselines Casa-Krakatau, -Knolls, and -Sherwin are based on extrapolation backward in time from January 1984. The length change in the baseline Casa-Lookout is determined from the Geodolite surveys (*12*). Symbols: (□) geodimeter station; (△) reflector station.

especially critical in the fit of the model to the two-color data.

The trial-and-error procedure that finally led to the development of model 2 (Fig. 1) entailed a change in the position of the deep inflation source to a point 4 km north and 2.3 km west of station Casa with an increase in depth to 14 km, the addition of a shallow inflation source near Casa Diablo hot springs as suggested by Rundle and Whitcomb (*7*), and an adjustment in the position of the south moat fault as well as an increase in the depth of slip to between 1 and 3 km. Although the initial trial position of the shallow inflation source was slightly west of station Casa and at a depth of 5 km (*7*), it was necessary, in view of the new data considered here, to move this source to a position 1 km north of station Casa and a depth of 6.5 km. In this model, each of the three sources contributes to the fit of the model to the data, all parameters being at least four times their standard errors. The parameters of model 2 that best fit the observations are 0.025 km^3 and 0.0021 km^3 of dilatation for the deep and shallow sources, respectively, and 62 mm of right lateral slip on the south moat fault.

In determining the parameters for models 1 and 2, the datum for the baseline Val-Lookout from the Geodolite data (*12*) was omitted because it contributed an exceptionally large residual. The fit of the new model to the combined data is acceptable (Table 2). Moreover, the sum of squared residuals for model 2 to the Geodolite data is as small as for model 1 (*13*).

We also tested models that, in addition to the sources contained in model 2, include an element intended to simulate dip-slip motion on a northern extension of the Hilton Creek fault into the caldera (*4, 14*). We conclude, however, that the inclusion of this additional source of deformation in the model is not warranted in that it did not provide a significant reduction in the residuals.

In summary, the two-color geodetic data indicate a high rate of network expansion, averaging approximately 3 ppm per annum between mid-1983 and late 1984. During this period, the rate of lengthening of nearly half of the 13 baselines for which data are available for the entire period decreased by factors of 2 to 3. The total deformation can be simulated reasonably well by means of two point sources of dilatation at depths of 14 and 6.5 km beneath the resurgent dome, in addition to shallow right lateral slip on the south moat fault. For the deep inflation source and the slip on the south moat fault, the parameters determined here, 0.025 km^3 and 62 mm, are consistent with those of Estrem and co-workers (*12*), who obtained 0.022 km^3 and 50 mm for the same time period.

It is difficult to establish how the deformation described here compares with the earlier deformation (*2*) because geodetic measurements of compatible resolution in space and time were not performed before mid-1983. The data from only a few of the Geodolite baselines that cover a longer period of time intimate a decrease in deformation rate for the mid-1983 to mid-1984 epoch compared to previous years (*12*). Although it is not necessarily valid to compare directly the parameters of model 2 to corresponding model parameters (*2, 7*) estimated from earlier data (*2*), it is nonetheless reasonable to conclude that substantially less slip (by about a factor of 4) occurred on the south moat fault during the mid-1983 to mid-1984 interval than during the previous 12 months, which included the intense January 1983 earthquake swarm and accompanying coseismic deformation.

In contrast to the decrease in deformation rate defined by the two-color data, Estrem and co-workers (*12*) have concluded that the data from monthly observations of six 1-km-aperture tilt arrays within the caldera and three 10-km-long trilateration lines that emanate from station Casa, measured to 0.8 μrad and 0.5 ppm standard error, respectively, can be adequately represented by linear rates of change for the mid-1983 to mid-1984 period. Most of their observations, however, lack the sensitivity necessary to resolve the decrease in deformation rate emphasized here. Of the tilt rates calculated from the leveling data, most are too low to enable a decrease by a factor of 2 to be detected within this time interval. Furthermore, only one of their three trilateration lines, Casa-Lookout, extended at a suffi-

Table 1. Summary of data and residuals to model 2 from measurements made with the two-color geodimeter for the interval 20 July 1983 to 10 August 1984.

Geodimeter station	Reflector station	L (km)	ΔL (mm)	σ* (mm)	Model 2 $(O\text{-}C)/\sigma_i$ (mm/mm)
Casa	Hot	6.85	7.01	1.53	−1.44
	Rodger	2.60	9.16	1.08	0.34
	Krakatau	7.80	18.0†	3.0†	−0.74
	Knolls	7.11	15.7†	2.7†	−2.24
	Lomike	2.49	9.25	1.08	0.01
	Sewer	3.94	16.56	1.19	0.56
	Sherwin	4.80	17.7†	1.9†	−2.71
	Miner	3.88	9.93	1.19	−0.08
	Slide	3.21	6.77	1.13	−2.00
	Tilla	4.16	0.43	1.22	0.05
	Shark	3.12	6.23	1.12	0.64
Miner	Tilla	4.91	21.86	1.29	2.76
	Shark	5.27	25.66	1.33	1.22
	Hot	9.68	25.26	1.92	−1.56
	Lomike	4.03	0.32	1.20	−0.28
	Sewer	4.12	0.37	1.21	0.66

*Standard error measurement of the length change based on the conservative assumption that ΔL is determined from only two measurements of the baseline (*9*). †Extrapolation based on parabolic trends fit to data from January 1984 to November 1984.

Table 2. The number of baselines and sum of squared residuals for the models.

Source	n	$\Sigma\,[(O\text{-}C)/\sigma_i]^2$	
		Model 1*	Model 2
Two-color data	16	1825.0	31.92
Geodolite	39	38.06*	35.04
Total	55	1863.0	66.95

*From Estrem and co-workers (*12*) with the Geodolite baseline Val-Lookout omitted.

ciently high rate to permit a decrease in rate of a factor of 2 to be detectable.

With the data at hand, it is not obvious which of the sources of deformation are implicated in the slowdown. The deceleration of the deformation sources cannot be spatially uniform because the decrease in deformation rate is spatially variable. However, simultaneous least-squares fitting of the distance measurements to model 2 at approximately bimonthly intervals indicates that no individual component of the model necessarily accounts for the observed deceleration. Nonetheless, the change in deformation rate detected by the two-color geodimeter is clearly discernible (Fig. 2) and must reflect changes in the level of activity at depth (*15*).

REFERENCES AND NOTES

1. J. C. Savage and M. M. Clark, *Science* **217**, 531 (1982); J. C. Savage and M. Lisowski, *J. Geophys. Res.* **89**, 7671 (1984); R. P. Denlinger and F. S. Riley, *ibid.*, p. 8303; R. O. Castle, J. E. Estrem, J. C. Savage, *ibid.*, p. 11507.
2. J. C. Savage and R. S. Cockerham, *J. Geophys. Res.* **89**, 8315 (1984).
3. C. H. Cramer and T. R. Toppozada, *Calif. Div. Mines Geol. Spec. Rep. 150* (1980), p. 91; A. S. Ryall and F. Ryall, *Science* **219**, 1432 (1983); C. O. Sanders, *J. Geophys. Res.* **89**, 8287 (1984).
4. R. A. Bailey, G. B. Dalrymple, M. A. Lanphere, *J. Geophys. Res.* **81**, 125 (1976).
5. A. H. Lachenbruch and J. H. Sass, *Geol. Soc. Am. Mem.* **152**, 209 (1978).
6. C. D. Miller, D. R. Mullineaux, D. R. Crandell, R. A. Bailey, *U.S. Geol. Surv. Circ. 877* (1982); D. P. Hill, R. E. Wallace, R. S. Cockerham, *Earthquake Predict. Res.* **3**, 551 (1985).
7. J. B. Rundle and J. H. Whitcomb, *J. Geophys. Res.* **89**, 9371 (1984).
8. By ranging on two optical wavelengths (red and blue) instead of just one, first-order corrections for variations in the speed of light along the path can be made, yielding distance measurements that are precise to about 0.1 ppm [L. E. Slater and G. R. Huggett, *J. Geophys. Res.* **81**, 6299 (1976)].
9. The instrument used to obtain these data is a new portable version of an observatory-based two-color ranging system that has been used to measure crustal deformation in California near Hollister [G. R. Huggett, L. E. Slater, J. O. Langbein, *J. Geophys. Res.* **82**, 3261 (1977)], Pearblossom (*10*), and most recently Parkfield [L. E. Slater and R. O. Burford, *Eos* **65**, 852 (1984)]. The long-term stability of the portable instrument has been assessed by conducting an extensive series of baseline measurements in parallel with the observatory-based system. For the time interval covered in this report, the only detectable change in the relative instrument scale occurred in the fall of 1983 and has been attributed to component replacements made during October 1983 in the portable instrument [J. O. Langbein, *U.S. Geol. Surv. Open-File Rep. 84-628* (1984), p. 220]. For our analysis, we adjusted the measured distances to account for this observed 0.43 ± 0.06 ppm increase in instrument length scale. Following J. C. Savage and W. H. Prescott [*J. Geophys. Res.* **78**, 6001 (1973)], we assumed the precision of the distance measurements to have the form $\sigma^2 = a^2 + b^2L^2$, where σ is the standard deviation of the error of a single distance measurement, L is the baseline length, and a and b are empirically determined constants. Using the least-squares technique, we fit parabolic functions of time to all the data presented here and determined that $a = 0.7$ mm and $b = 0.12$ ppm. This error budget appears to be independent of the averaging interval for periods of 3 to 15 months and is consistent with corresponding results obtained from the intercomparison tests with the observatory-based instrument.
10. J. O. Langbein, M. F. Linker, A. McGarr, L. E. Slater, *Science* **218**, 1217 (1982).
11. J. C. Savage, W. H. Prescott, M. Lisowski, N. E. King, *J. Geophys. Res.* **86**, 6991 (1981).
12. J. E. Estrem, M. Lisowski, J. C. Savage, *J. Geophys. Res.* **90**, 12683 (1986).
13. Although estimates of vertical deformation within the caldera for this interval (*12*) are qualitatively consistent with uplift of the resurgent dome as predicted by either of the models, both models fail the χ^2 test when compared to computed tilt rates alone. However, this inconsistency is neither surprising nor fatal in that vertical geodetic data from volcanic regions are commonly incompatible with simple models constructed to conform with horizontal geodetic data alone [J. H. Dieterich and R. O. Decker, *J. Geophys. Res.* **80**, 4094 (1975)]. With the inclusion of additional model parameters, the degree of model misfit could be improved.
14. G. C. Taylor and W. A. Bryant, *Calif. Div. Mines Geol. Spec. Rep. 150* (1980), p. 49.
15. K. Mogi, *Bull. Earthquake Res. Inst. Tokyo* **36**, 99 (1958).

16. We thank P. Bozek, G. Burton, J. E. Estrem, K. Hudnut, D. Knapp, E. A. Lawrence, P. Levine, M. L. MacKenzie, M. Mann, V. Pease, D. B. Reneau, and A. J. Rigoni for their participation in the field operations; M. D. Clark for support in initiating the field program; L. E. Slater and R. O. Burford for cooperating in the intercomparison tests, which began in early 1980; J. C. Savage for the use of his program for modeling dislocations in an elastic half-space and for early access to the Geodolite data; and D. P. Hill, W. H. Prescott, J. C. Savage, and M. Lisowski for helpful discussions.

24 June 1985; accepted 26 Nover[illegible] 1985

Geometrical Aspects of Sorted Patterned Ground in Recurrently Frozen Soil

KEVIN J. GLEASON, WILLIAM B. KRANTZ, NELSON CAINE, JOHN H. GEORGE, ROBERT D. GUNN

A model for sorted patterned ground shows that some types arise from density-driven Rayleigh free convection that occurs during thawing of water-saturated recurrently frozen soils. The regularly spaced convection cells result in an uneven melting of the underlying ice front. Frost action causes stones to be upthrusted and to form in a pattern on the ground surface that mirrors the corrugation in the underlying ice front. The implications of the water circulation direction in the cells on the sorting process are considered.

"SORTED PATTERNED GROUND" refers to symmetrical forms such as polygons (Fig. 1) or stripes (Fig. 2) that are made prominent because of the segregation of stones and fines resulting from diurnal, seasonal, or other recurrent freeze-thaw cycles in water-saturated soils. These patterns can be found underwater (Fig. 3) as well. A model developed by Ray *et al.* (*1, 2*) explains many features of a broad class of patterned ground. We present new data in support of this model and report further model development describing pattern geometry.

Rayleigh free convection (*3*) is the basis of the model of Ray *et al.* When frozen soil thaws, the potential for free convection exists at least during some portion of the thaw period because of the density inversion for water between 0° and 4°C (*4*). That is, more dense water a few degrees above its freezing point can overlie less dense water at 0°C. A linear stability analysis permits one to determine the conditions necessary for the onset of free convection [that is, the critical Rayleigh number (*5*)]. The model of Ray *et al.* differs substantively from earlier free convection models (*6–8*) that assume that the weak convection currents can move either the stones or the soil; this assumption has been shown to be physically unrealistic (*9*). Ray *et al.* assumed that the fluid flows through the soil and stone mixture. Once Rayl[illegible] convection occurs (*10*), it typically forms hexagonal flow cells in horizontal ground and roll cells or helical coils in sloped terrain. These regular cellular flow patterns can then be impressed on the underlying ice front as shown in Fig. 4, because in areas of downflow, the warmer descending water causes preferential melting. In areas of upflow, the rising cooler water hinders melting of the ice front. Consequently a pattern of regularly spaced peaks and troughs is formed in the underlying ice front that mirrors the polygonal or striped cellular convection patterns in the thawed layer. This pattern is transferred to the ground surface through the process of sorting by well-established mechanisms such as frost push or frost pull (*11*). That is, a freeze-thaw cycle causes the stones to be heaved upward relative to the ice peaks and troughs. This leads to polygonal (predominantly hexagonal) stone patterns for polygo-

K. J. Gleason and W. B. Krantz, Department of Chemical Engineering, University of Colorado, Boulder, CO 80309.
N. Caine, Department of Geography and Institute for Arctic and Alpine Research, University of Colorado, Boulder, CO 80309.
J. H. George, Department of Mathematics, University of Wyoming, Laramie, WY 82071.
R. D. Gunn, Department of Chemical Engineering, University of Wyoming, Laramie, WY 82071.